Experimental Investigation and Simulation of Al–Si Casting Microstructure Formation

Adnan S. Jabur, Jalal M. Jalil & Ayad M. Takhakh

Arabian Journal for Science and Engineering

ISSN 1319-8025

Arab J Sci Eng
DOI 10.1007/s13369-012-0189-2

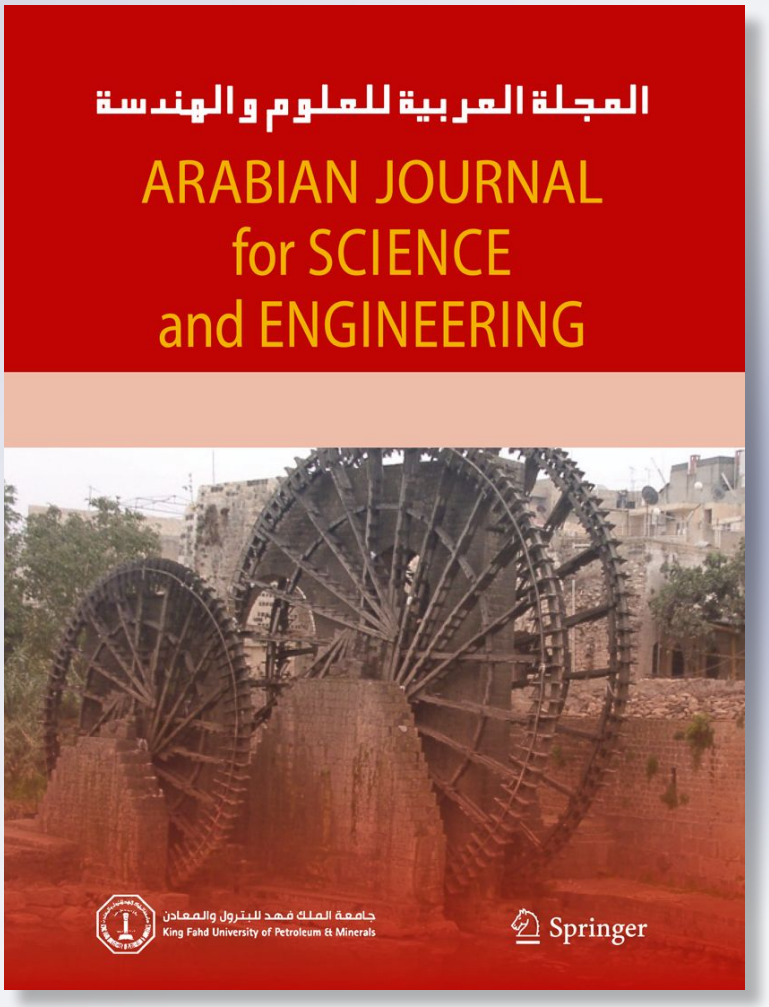

Springer

Arab J Sci Eng
DOI 10.1007/s13369-012-0189-2

RESEARCH ARTICLE - MECHANICAL ENGINEERING

Adnan S. Jabur · Jalal M. Jalil · Ayad M. Takhakh

Experimental Investigation and Simulation of Al–Si Casting Microstructure Formation

Received: 24 September 2009 / Accepted: 10 July 2010

Abstract The aim of the present study is to investigate the influence of thermal variables on the as-cast microstructure of hypoeutectic and eutectic Al–Si alloys and to establish correlation between the solidification thermal parameters and interparticle spacing for Al–12%Si alloy during the unidirectional solidification. New relationships are suggested based on the image processing programs in order to accurately quantify the microstructure evolution. A numerical approach is developed to quantitatively determine solidification thermal variables such as growth rate (interface velocity), temperature gradient, cooling rate, and local solidification time. The experimental microstructure measurements are combined with numerical solutions using finite difference (FD) and control volume (CV) methods, and models are obtained for this structure with solidification parameters. Applying image processing program with relationships suggested in this study gives more accuracy to compute interparticle spacing compared with conventional methods. For Al–12%Si alloys, which are widely used, the dispersion of the phases must reflect both decreasing interface velocity and temperature gradient as the microstructure is examined from the chilled surface towards the riser, thus, increasing coarseness of the microstructure caused by both factors.

Keywords Casting · Simulation · Finite volume · Finite difference · Eutectic Al–Si alloy

الخلاصة

تهدف هذه الدراسة إلى بيان تأثير الخواص الحرارية على البنية الدقيقة لمسبوكات المنيوم – سليكون اليوتكتيك و قبل اليوتكتيك وإنشاء علاقة متبادلة بين المتغيرات الحرارية للتجمد مع المسافة بين الدقائق لسبيكة المنيوم – 12% سليكون خلال التجمد ذي الاتجاه الواحد. لقد تم اقتراح علاقات جديدة لغرض حساب البنية الدقيقة بالاعتماد على البرامج الحديثة لمعالجة الصور الرقمية بصورة اكثر دقة. كما تم تطوير الطرق العددية لتحديد متغيرات التجمد مثل معدل النمو (سرعة الحد الفاصل)، والانحدار الحراري، ومعدل التبريد و زمن التجمد الموضعي. ومن خلال التوافق بين القياس العملي للبنية الدقيقة والحلول العددية تم الحصول على نماذج لهذه البنية مع متغيرات التجمد. إن تطبيق برنامج معالجة الصور مع العلاقات المقترحه في هذه الدراسة يعطي دقة أكثر في حساب المسافة الطبقية بالمقارنة مع الطرق التقليدية. إن المسافة بين الدقائق لسبائك المنيوم – 12% سليكون تعتمد كثيرا على النقصان في كل من سرعة الحد الفاصل والانحدار الحراري عندما تقاس البنية من سطح المصقع باتجاه المغذي وبذلك فإن الزيادة في خشونة البنية الدقيقة ينتج بسبب كلا العاملين.

A. S. Jabur
Mechanical Engineering Department, College of Engineering, Basrah University, Basrah, Iraq

J. M. Jalil (✉)
Electromechanical Engineering Department, University of Technology, Baghdad, Iraq
E-mail: jalalmjalil@yahoo.com

A. M. Takhakh
Mechanical Engineering Department, College of Engineering, Al-Nahrain University, Baghdad, Iraq

Published online: 17 February 2012

List of Symbols

Cp	Specific heat (J/kg K)
E	Enthalpy (J/kg)
f	Fraction of phase
G	Temperature gradient (°C/mm)
h	Heat transfer coefficient (W/m^2 K)
K	Thermal conductivity (W/m K)
L	Latent heat (J/kg)
R	Cooling rate (°C/s)
S	Coefficient in Eq. (3)
T	Temperature (°C)
T*	"Kirchhoff" temperature (factor) (W/m)
T_L	Liquidus temperature (°C)
T_S	Solidus temperature (°C)
t	Time (s)
V	Interface velocity "Growth velocity" (mm/s)
x, y, z	Cartesian coordinates
α	Thermal diffusivity (m^2/s)
Γ	Coefficient in Eq. (3)
λ	Inter-particle spacing (mm)
ρ	Density (kg/m^3)

1 Introduction

It is well understood that the freezing front velocity (V) and the temperature gradient (G) are important solidification parameters that determine the structure of cast products. The ratio G/V determines the type of growth morphology (dendritic, cellular, or eutectic). The control of interface temperature gradient (G) and interface velocity (V) is therefore established as a design objective. This paper shows that how the eutectic solidifies and the resulting morphology depends on many parameters. The effect of the thermal gradient and growth velocity is important and has been studied extensively using directional solidification experiments with Bridgman-type furnaces. Several models have been proposed to quantify the effect of cooling conditions on the eutectic microstructure and growth temperature [1]. The difficulty associated with the modeling of solidification processes arises from both the morphological complexity, and the range of length- and time-scales [2,3].

This paper describes micro-structural modeling of irregular Al–Si alloys at eutectic compositions. Two models, a finite difference-temperature model (FD-TM) and a control volume-enthalpy model (CV-EM), are used to describe the thermal field and microstructure evolution for alloy systems as a function of interface velocity (V), temperature gradient (G), and cooling rate (R). The accurate measurement of interface undercooling in anomalous eutectic solidification is made difficult by the need to impose a high temperature gradient to produce an approximately isothermal interface. Borland and Elliot [4] specify a planar solid–liquid interface and an almost zero temperature gradient so that the interface is highly isothermal, and at high gradients the change of slope as the interface passes the thermocouple bead becomes imperceptible [5].

2 Governing Equations

2.1 Model (A): Finite Difference-Temperature Model (FD-TM)

The simulation of casting involves thermal and stress analysis. The thermal analysis requires the solution of the energy balance equation (1). This equation must be solved for the casting and the mold to find the temperature history at every point in the casting, T(x, y, z, t) [6].

$$\frac{\partial}{\partial X}\left(k_X\frac{\partial T}{\partial X}\right)+\frac{\partial}{\partial Y}\left(k_Y\frac{\partial T}{\partial Y}\right)+\frac{\partial}{\partial Z}\left(k_Z\frac{\partial T}{\partial Z}\right)+Q=\rho C_P\left(\frac{\partial T}{\partial t}+V_X\frac{\partial T}{\partial X}+V_Y\frac{\partial T}{\partial Y}+V_Z\frac{\partial T}{\partial Z}\right) \quad (1)$$

where: k_X, k_Y, k_Z are the thermal conductivity, C_p is the specific heat, ρ is the density, Q is the heat source, V_X is the flow velocity in X direction, V_Y is the flow velocity in Y direction, V_Z is the flow velocity in Z direction.

We assume that if the flow of molten metal is not considered; all velocity terms are effectively zero. The very small variation in the spatial terms on the right hand side of Eq. (1) justifies this approximation. In the simulation, the latent heat is assumed to be released linearly between the solidus and liquidus temperatures. Using these assumptions, Eq. (1) is simplified to Eq. (2) [7].

$$k\left(\frac{\partial^2 T}{\partial X^2}+\frac{\partial^2 T}{\partial Y^2}+\frac{\partial^2 T}{\partial Z^2}\right)+Q=\rho C_P\frac{\partial T}{\partial t}$$
$$\mathrm{Q}=\rho \mathrm{L}\frac{\partial f_s}{\partial t} \tag{2}$$

where f_s is the solid fraction and L is the volumetric latent heat.

These equations are for the mushy region, and therefore are written without a source term (Q) for the solid and liquid regions.

The primary difference between macro- and micro-models is in how the local fraction of solid (f_s) is computed [8].

To solve Eq. (2), a relationship between the field T and f_s must be found. A simple and widely used approach assumes that the fraction of solid f_s depends only on the temperature T and not upon cooling rate or growth rate. For pure metal or eutectic alloys, one can assume that $f_s = 0$ above the melting point or the eutectic temperature and that $f_s = 1$ below the equilibrium temperature.

2.2 Model (B): Control Volume-Enthalpy Model (CV-EM)

For most of the process of alloy solidification, there is no clear boundary between the liquid and solid. Instead, the mushy zone, which has a solid fraction from zero to unity, is present. For this case, the enthalpy method is more appropriate. The conservation of energy equation in the enthalpy method is considered in terms of enthalpy (E) instead of temperature [9], the governing equations are based directly on the model proposed by Cao et al. [10]

$$\frac{\partial(\rho E)}{\partial t}=\frac{\partial^2(\Gamma E)}{\partial X^2}+\frac{\partial^2(\Gamma E)}{\partial Y^2}+\frac{\partial^2(\Gamma E)}{\partial Z^2}+P$$
$$P=\frac{\partial^2 S}{\partial X^2}+\frac{\partial^2 S}{\partial Y^2}+\frac{\partial^2 S}{\partial Z^2} \tag{3}$$

$\Gamma = \Gamma(E)$, $S = S(E)$, coefficients.

The energy equation has been transformed into a non-linear equation with a single dependent variable E. The non-linearity of the phase change problem is evident in the above equation.

In the liquid region, Eq. (3) is reduced to the normal linear energy equation.

$$\frac{\partial(\rho_L E)}{\partial t}=\frac{\partial}{\partial X}\left(k_L\frac{\partial T}{\partial X}\right)+\frac{\partial}{\partial Y}\left(k_L\frac{\partial T}{\partial Y}\right)+\frac{\partial}{\partial Z}\left(k_L\frac{\partial T}{\partial Z}\right) \tag{4}$$

Also, in the solid region Eq. (3) reduces to

$$\frac{\partial(\rho_S E)}{\partial t}=\frac{\partial}{\partial X}\left(k_S\frac{\partial T}{\partial X}\right)+\frac{\partial}{\partial Y}\left(k_S\frac{\partial T}{\partial Y}\right)+\frac{\partial}{\partial Z}\left(k_S\frac{\partial T}{\partial Z}\right) \tag{5}$$

Enthalpies of the liquid and solid phases are given by: [6]

$$\mathrm{E_L}=\mathrm{C_L T}+\mathrm{E_{L0}} \tag{6}$$
$$\mathrm{E_S}=\mathrm{C_S T} \tag{7}$$

where E_{L0} is the reference enthalpy expressed as

$$\mathrm{E_{L0}}=(\mathrm{C_S}-\mathrm{C_L})\mathrm{T_{eut}}+\mathrm{E_f} \tag{8}$$

and E_f is the enthalpy of fusion at the eutectic temperature T_{eut}. Using Eqs. (6), (7) and (8), the mixture enthalpy is expressed in terms of temperature as:

$$\mathrm{E}=\mathrm{fE_L}+(1-\mathrm{f})\mathrm{E_S}=\mathrm{f}\left[(\mathrm{C_L}-\mathrm{C_S})(\mathrm{T}-\mathrm{T_{eut}})+\mathrm{E_f}\right]+\mathrm{C_s T} \tag{9}$$

The Linear rule is used to calculate the solid fraction and is given by

$$f_s = 1 - \left(\frac{T - T_S}{T_L - T_S}\right)$$

3 Thermophysical Alloy Data

Most commercial casting simulation packages solve the equations of heat transfer to produce solidification results. With this being the case, the most important simulation parameters are those which control heat transfer. The important alloy parameters are the metal density (ρ), specific heat (C_p), thermal conductivity (k), latent heat (L), and solid fraction (f_s).

All of these parameters are a function of temperature. Some of these properties do not change appreciably from one alloy composition to another, allowing the parameter to be generalized for a certain class of alloy [11]. Table 1 shows constant thermophysical properties for Al–12%Si.

4 Experimental Methods

Al–Si eutectic alloys were selected, Table 2 gives the details of composition of the alloys.

Figure 1 shows the experimental setup. During metal cooling and freezing, the temperature was measured in the casting at three different locations, 30, 50 and 90 mm from chill/metal interface. Typical experimental results were compared to those numerically simulated by using finite difference (FD) and control volume (CV) methods to verify the accuracy of the simulation results. The cooling curves were measured using three K-type thermocouples. The thermocouples were calibrated at the melting temperatures of tin, lead, and aluminum. The calibration graph is shown in Fig. 2.

4.1 Inter-Particle Spacing Calculation

To calculate inter-particle spacing for Al–12%Si, the following relationships can be applied:

$$\lambda_p = \sqrt{\frac{Image\ldots area}{Particals\ldots number}} \quad \text{(Pixel)} \tag{10}$$

where λ_p is the inter-particle spacing in an image with pixel unit = 0.27 mm = 270 μm

Table 1 Constant thermophysical properties for Al–12%Si

Symbol	Property	Quantity	Unit
ρL	Liquid density	2,482	kg/m^3
ρS	Solid density	2,680	kg/m^3
kL	Liquid thermal conductivity	64	W/m K
kS	Solid thermal conductivity	139	W/m K
CPL	Liquid specific heat	1,190	J/kg K
CPS	Solid specific heat	860	J/kg K
TL	Liquidus temperature	575 (for FD) –	°C
TS	Solidus temperature	565 (for FD) 577 (for CV)	°C
TP	Pouring temperature	650	°C
L	Latent heat	413,000	J/kg
ko	Partition ratio	0.132	/

Table 2 Composition of Al–Si alloys

Alloy type	wt% Si	wt% Fe	wt% Cu	wt% Mn	wt% Mg	wt% Zn	wt% Ti	wt% Al
Al–12%Si (Binary)	12	0.5	–	–	–	–	–	Balance
A413 (LM6)	10.5–13.5	0.55	0.05	0.35	–	0.1	0.15	Balance

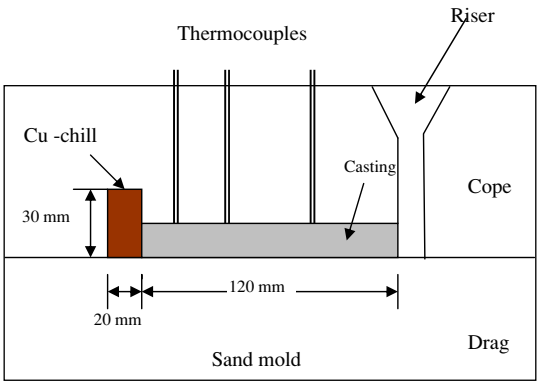

Fig. 1 Experimental setup

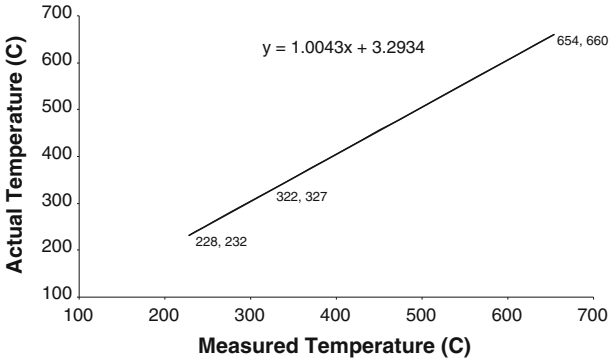

Fig. 2 *Calibration curve* for the K-type thermocouples

So that the real spacing is λ is:

$$\lambda = \frac{\lambda_p * 270}{M} \tag{11}$$

where: λ is the real inter-particle spacing in μm, M is the magnification power.

4.2 Results and Discussion

A combination of numerical and experimental approaches is developed to quantitatively study the solidification thermal parameters of interface velocity, temperature gradient, and cooling rates during unsteady-state solidification of eutectic Al–Si alloys.

Studies of the effect of solidification variables on microstructure of casting are important because the as-solidified microstructure dictates heat treatment and the final mechanical performance of the casting. The interphase (inter-particle) and dendritic spacing are important micro structural parameters resulting from the solidification process.

The results of the experimental thermal analysis of casting are compared with simulations using finite difference (FD) and control volume (CV) methods. A good agreement has been obtained between the simulation curves and the experimental values. Figure 5 shows the validation for results from Al–12%Si alloy taken at three locations −30, 50, and 90 mm in the casting from chill/cast interface.

The numerical models were applied to simulate the solidification eutectic alloys in a rectangular mold cavity using a copper chill to obtain unidirectional solidification. These models are used to calculate solidification thermal parameters such as: interface velocity (or tip-growth-rate) (V), temperature gradient (G), cooling rate (R), and local solidification time (t_f). These are explicitly calculated at each time increment (0.01 s) of the simulation. Figures 4, 5, 6 and 7 show typical numerical results for cooling curves, solidification parameters as a function of position (p) from metal/chill interface, and temperature distribution in cavity with time.

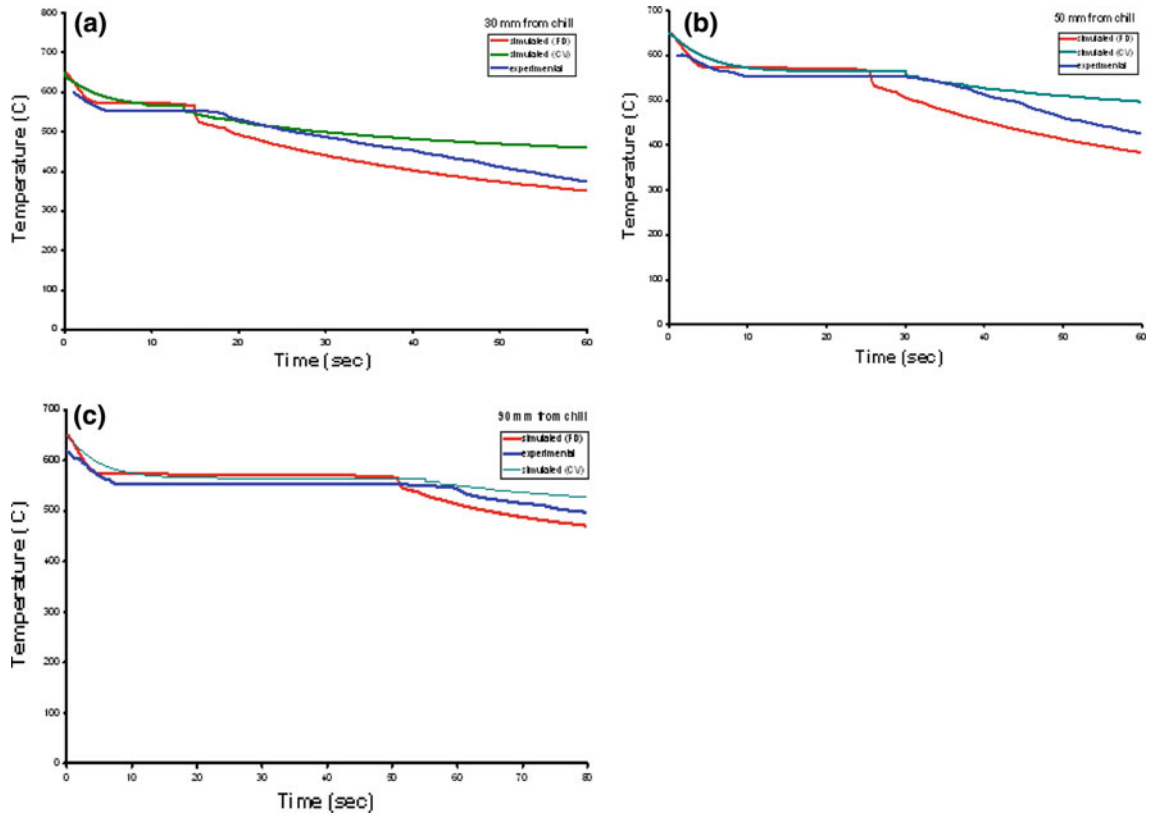

Fig. 3 The verification results, **a** at 30 mm from chill/cast interface, **b** 50 mm, **c** 90 mm

The relationship between these thermal features indicates a similar solidification process for both alloys under analysis, with very close profile matches for these parameters as a function of position (P) from metal/chill interface. The thermal variable power laws [V = f(P) and R = f(P)] which characterize solidification along the castings are the same for eutectic Al–Si alloys, and the particle spacing is dependent on the thermal solidification variables.

The cooling curve of the Al–12%Si alloy at different positions along the casting is shown in Fig. 3. It is clear from this figure that the solidification time is very short near to the chill/cast interface and then the time increases to the end of casting. The degree of difference in cooling curve behavior at different positions along the casting is related to the differences in cooling rate.

As a result of using the copper chill, the cooling rate will be very high at the chill/cast interface region and then will decreases until a distance of approximately 50 mm is reached, as shown in Fig. 4. The constancy of cooling rate can be clearly seen beyond a distance of 50 mm. This increase in the cooling rate leads to a modification in the microstructure of Al–12%Si alloy which in turn improves the mechanical properties.

The relationship between temperature gradient and distance at different positions along the casting is shown in Fig. 5. It is important to notice that the temperature gradient is high in the region adjacent to the copper chill. Figure 5 also shows that the lateral temperature gradient is very little changed at the mold wall compared to the center of the casting. This is because the mold wall acts as an insulator during solidification. The mould wall does not has the ability to act as a chill through all stages of solidification because of the greater thickness of the insulative sand mould wall compared with the volume of the molten metal.

The effect of chill on the behavior of the interface velocity (Fig. 6) is the same as on the cooling rate, being very high near the chill/cast interface region and then decreasing until a distance of approximately 50 mm is reached.

Figure 7 represents the distribution of local solidification times. There is a linear relationship between local solidification time and the distance from chill/cast interface toward the riser because of the verified directional solidification for these alloys. This validates the application of the results of this simulation in micro structural

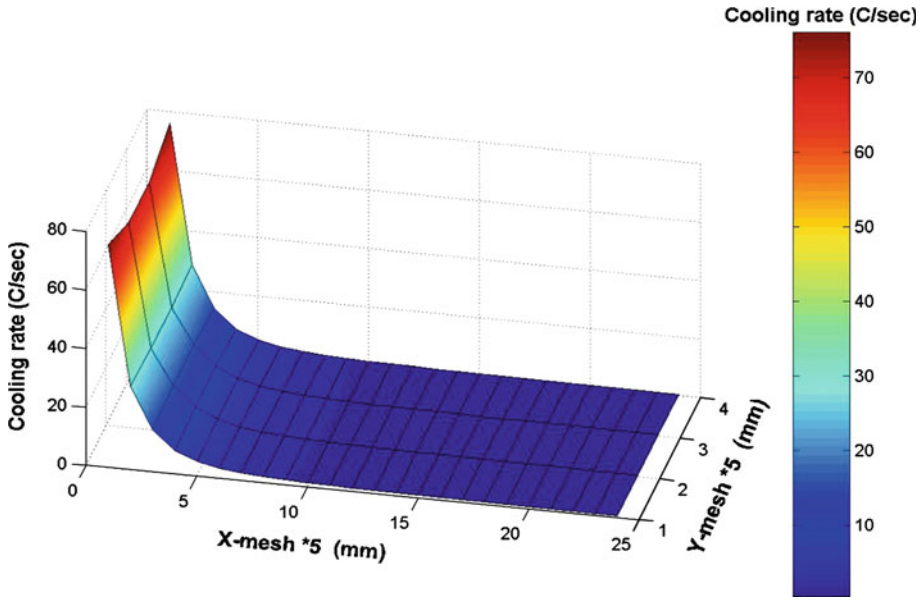

Fig. 4 The distribution of cooling rate through the mid surface (X–Y)

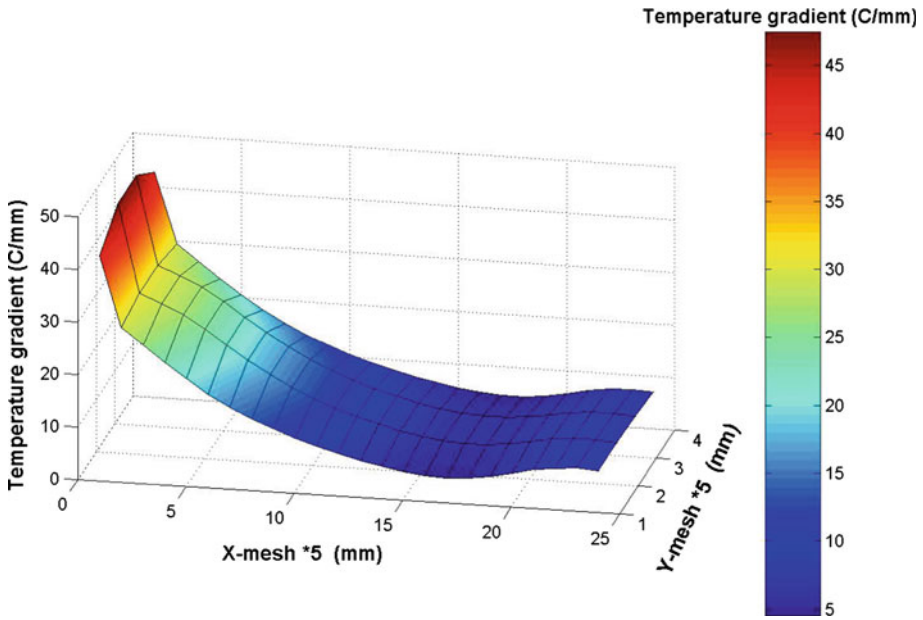

Fig. 5 The distribution of temperature gradient through the mid surface (X–Y)

modeling for the Al–Si alloys used, as an alternative to conventional methods used in previous studies such as the Bridgman furnace.

The use of this type of solidification simulation and the use of variable properties for each phase with temperature, gives a significant improvement in accuracy.

The main advantage of a simulation model is that it facilitates calculation and clarifies the effect of each variable. It is thus possible to plot curves which indicate the effect of varying the alloy properties upon the inter-particle spacing.

Cooling curves at different locations of a middle (x, y) surface are calculated using a solidification simulation program based on finite difference (FD) and control volume (CV) methods.

The predicted cooling curves are compared in Fig. 8 for different locations from chill/cast interface for Al–12%Si alloy.

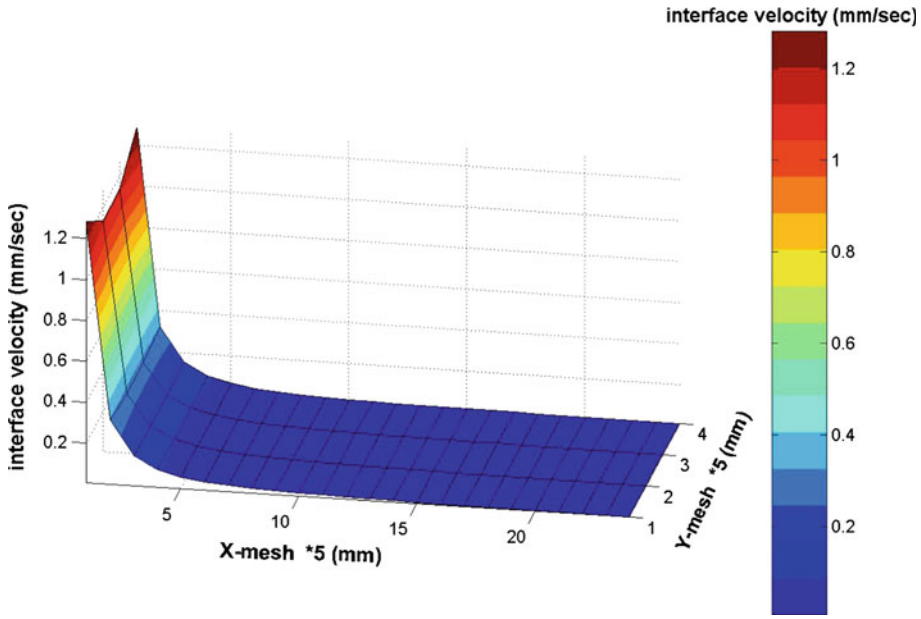

Fig. 6 The distribution of interface velocity through the mid surface (X–Y)

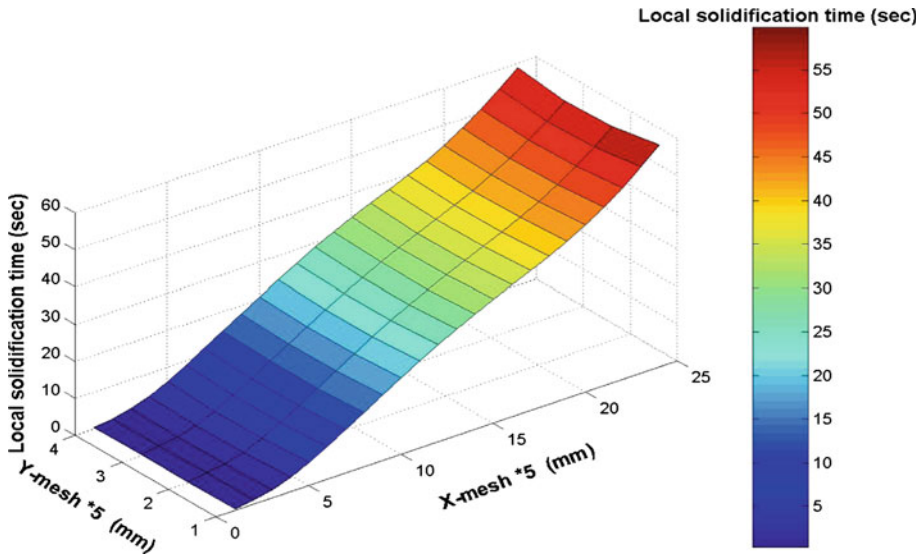

Fig. 7 The distribution of local solidification time through the mid surface (X–Y)

From Figs. 3, 8 and 9, the enthalpy transforming model (i.e. CV-EM) proposed in this study proves to be capable of handling complicated phase change problems occurring at a single temperature with fixed grids. Comparisons made between the numerical results from the finite difference method and experimental results show good agreement, showing that the present model can properly predict the phase change processes. The advantage of this enthalpy based model is that it does not require an explicit description of the nature of the phase change front.

4.3 The Study of Microstructure of Al–12%Si

The inter-particle spacing (λ) was measured from photographs. Figure 10 explains the sequence of image treatment from original photo to final image using Al–12%Si as an example. Figure 11 shows the image processing method, where λ was measured from a longitudinal section in different regions. Figures 12, 13, 14,

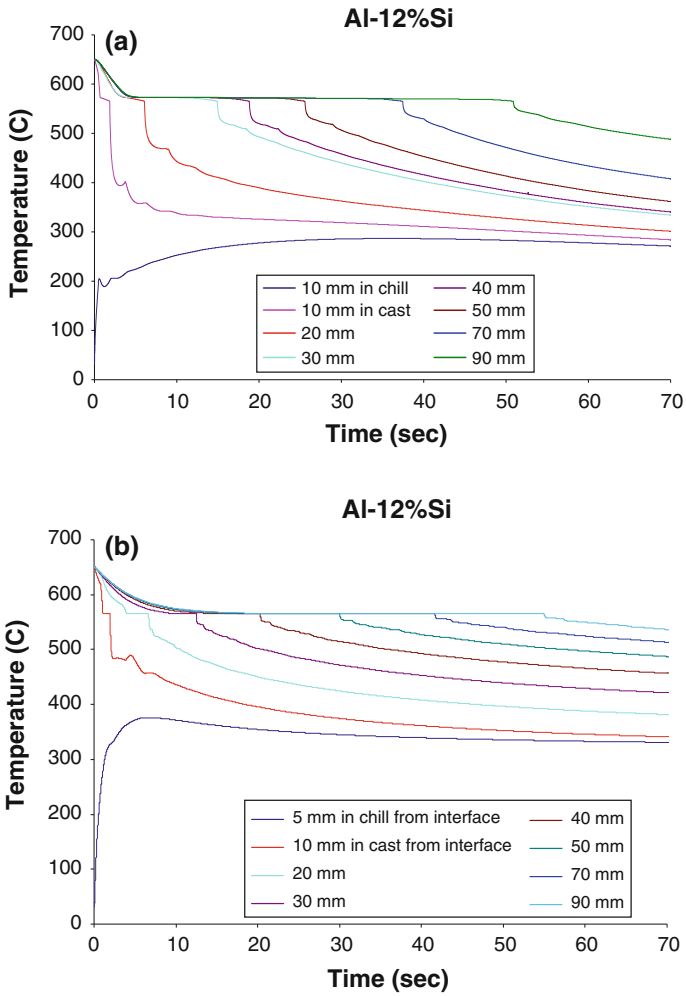

Fig. 8 Cooling curves and heating curves for Al–12%Si. **a** Finite difference, **b** control volume

and 15 show the relationship of average inter-particle spacing (λ) obtained from image processing and thermal parameters, which are obtained from the simulations.

It has been observed that there are differences in the measurements of the inter-particle spacing and the relationship with practical and theoretical measured variables. These differences are related to the differences in the method of measuring and numbers of particles measured.

It is to be expected that an increase in the number of calculated particles for, as an example, the linear intercept method and taking the average, leads to greater accuracy, because of the random distribution and size of particles in Al–Si alloys. In spite of difficulty of scanning every or even most of the particles on the inspected surface, it has become possible, by using image processing of the type described here, to cover all the inspected surface and to measure average inter-particle spacing, average size, and particle distribution. Therefore it is to be expected that the method used in this study combined with solidification simulation gives better results than those of the conventional method used in previous studies.

The reason why researchers refrain from studying irregular eutectics is the relationship between inter-particle spacing (λ) with solidification parameters (such as V, G, and R) is difficult to measure experimentally over a sufficient area of the casting, because a very large number of thermocouples must be installed and read. Some studies have used a special growth furnace or a Bridgman furnace to control growth rate or a small number of thermocouples which may not cover a sufficient area of the casting.

We use simulation to obtain a temperature history for any region or node of the casting, thence solidification parameters (V, G, R) and local solidification time (t_f) can be calculated. The accuracy of the simulation is verified by comparison with experimental data (T- t curve) as shown in Fig. 3. The comparison

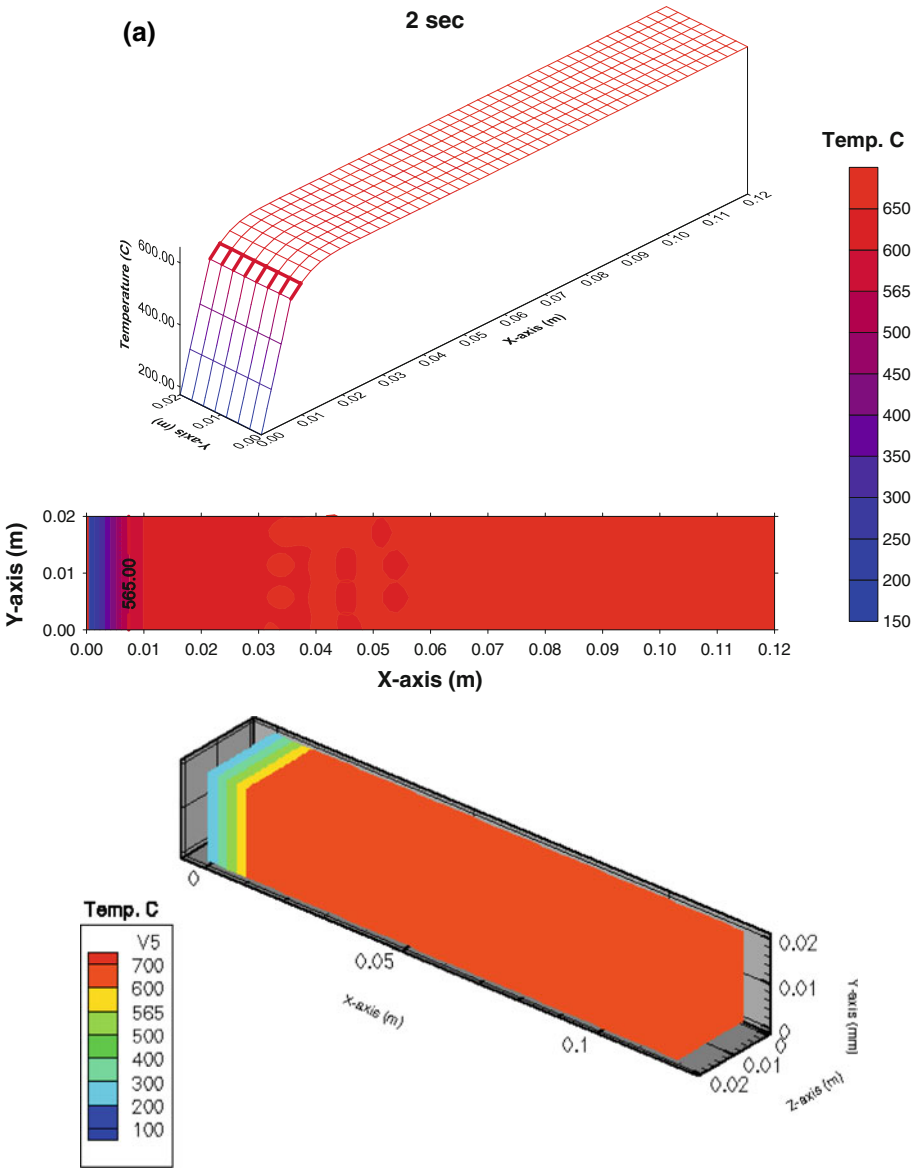

Fig. 9 Contours, surfaces, and solids temperature distribution in cavity shows the motion of the solid/liquid interface over time for Al–12%Si. **a** 2 s, **b** 10 s, **c** 40 s

confirms simulation results, which effectively mimic the presence of thousands of thermocouples inside the casting.

At lower velocities, the structure consists of thick Si plates, as shown in Fig. 11c, d, surrounded by a thick Al halo. Much finer Si flakes grow in the depressions between the coarse plates: this structure is shown in Fig. 11a, b. As the velocity increases the interface becomes more planar and the flake morphology dominates the structure. However, the coarse silicon does not disappear completely from the structure even at velocities greater than 500 μm/s and the silicon particles form a fibrous morphology. These observations show that the interface structure is different at low and high velocities.

Eutectic growth calculations, using solidification simulation, indicate the following relationship of interface velocity (V) with inter-particle spacing (λ) (see also Fig. 15):

$$\lambda = 0.0043\mathrm{V}^{-0.3418}.$$

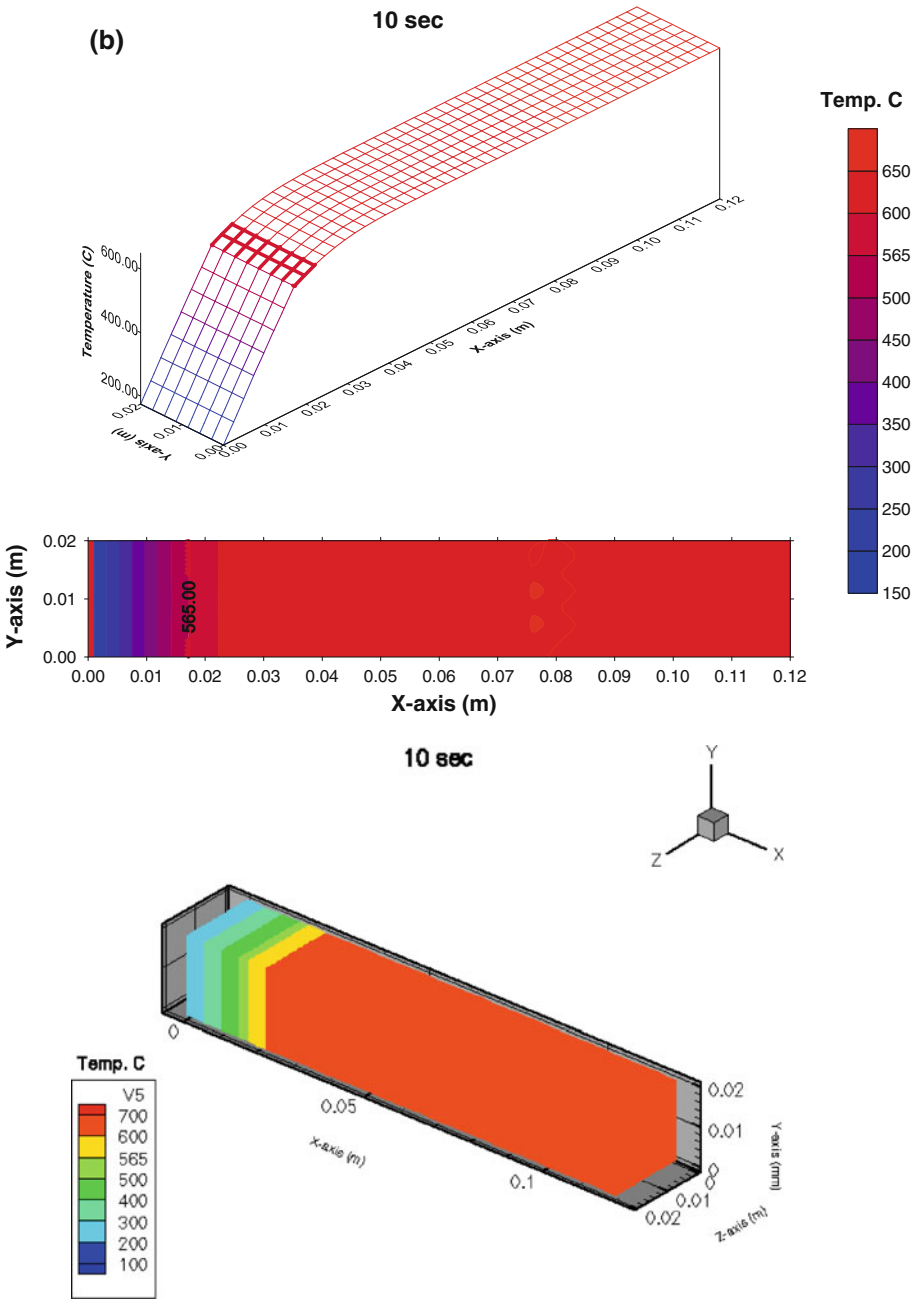

Fig. 9 continued

The influence of temperature gradient in the liquid is related to its effect on flattening the solid-liquid interface. This makes solute rejection from the Si flake tip more difficult, promoting morphological instability, increasing the frequency of branching and reducing the average interflake spacing. This reduced spacing promotes diffusion.

However, as Fisher and Kurz [13] comment, the analysis is approximate, assuming a $\lambda - V^{0.5}$ dependence and containing many system parameters, and within the framework of the analysis, allowing for the under-cooling to increase with temperature gradient. Unfortunately as yet, few structural observations and quantitative measurements have been made as a function of temperature gradient, but the spacing does actually decrease with increasing temperature gradient, as illustrated in Fig. 13.

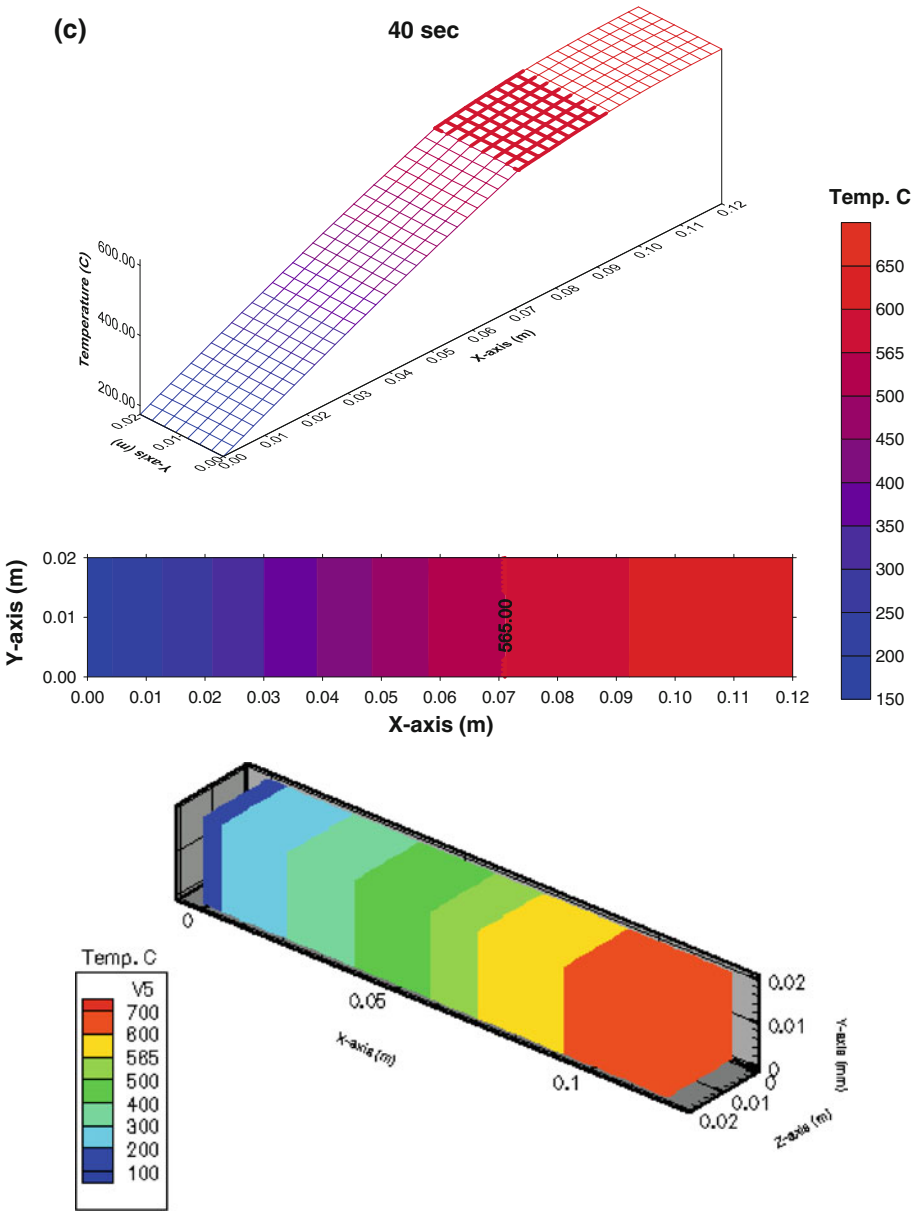

Fig. 9 continued

To further reinforce this conclusion, an attempt was made to correlate $\lambda^2 V$ as a function of G. If a relationship of the form $\lambda^2 V = \text{constant } G^n$ does exist, then a logarithmic plot of $\lambda^2 V$ versus G should yield a straight line with slope n. Figure 15 shows $\lambda^2 V$ as a function of G. A linear regression analysis of this data yielded a value of -0.7612 for n. Figure 15 shows a good agreement between the current study and results from Toloui and Hellawell [12] and Fisher and Kurz [13]. The percentage difference in the results between the present study and Fisher and Kurz is nearly 30% while the difference percentage in results between the present study and Toloui and Hellawell [12] is nearly 10%. Both these percentages are acceptable differences for time comparison.

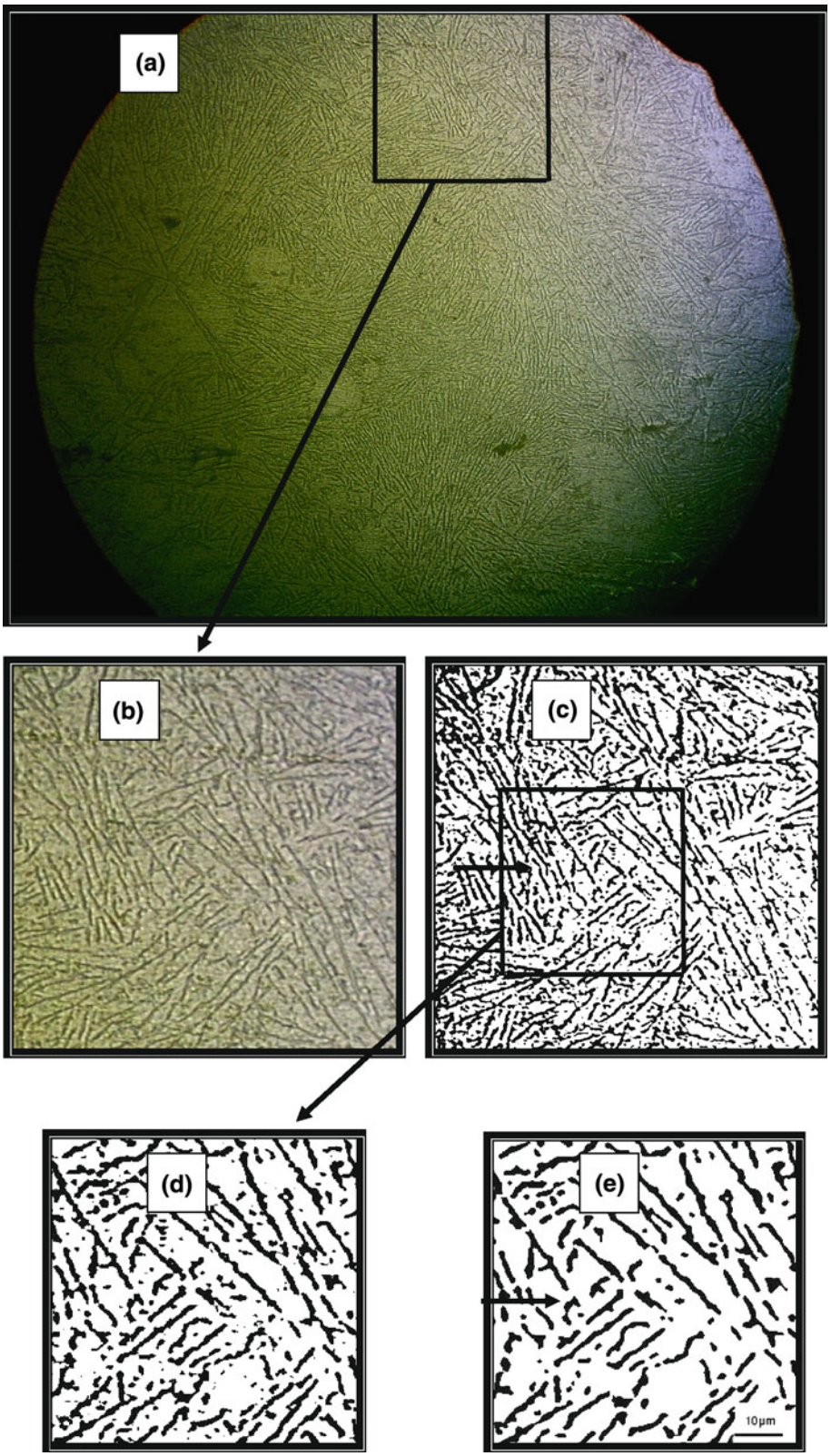

Fig. 10 Sequence of image treatment for distance 20 mm from chill of Al–12%Si alloy; **a** original, **b** sub select-1, **c** threshold, **d** sub select-2, **e** final image after filtration and processing

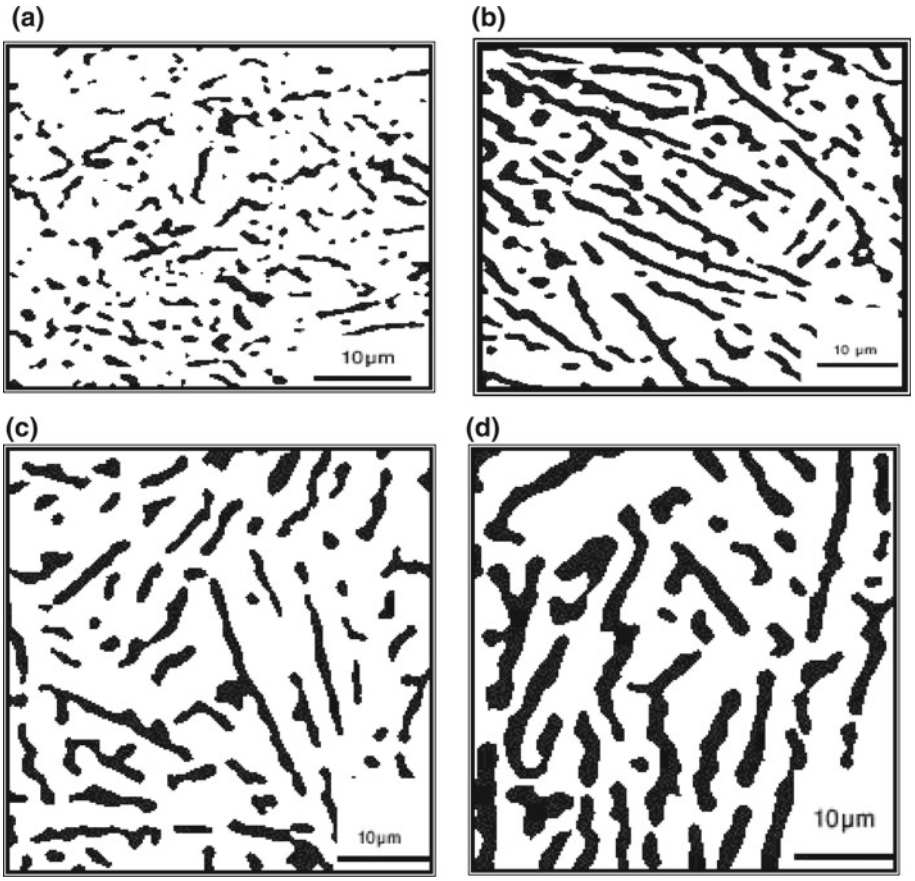

Fig. 11 Structure variation of Al–12%Si along the casting at the following distances from the chill, **a** 10 mm, **b** 30 mm, **c** 60 mm, **d** 100 mm

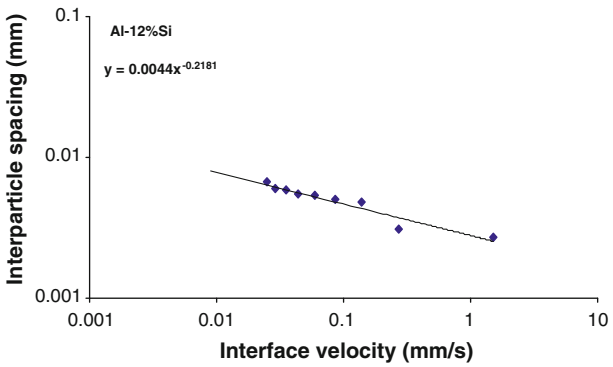

Fig. 12 Relationship between inter-particle spacing (λ) and interface velocity (V) for Al–12%Si

5 Conclusions

1. Applying image processing to examine the relationships suggested in this study improves the accuracy of the calculation of inter-particle spacing for irregular Al–Si alloys compared with conventional methods.
2. A new model describes irregular eutectic spacing in Al–12%Si alloys. The spacing is a function of growth rate and temperature gradient and the resulting equation after linear regression is:

$$\lambda^2 V = 5\mathrm{E} - 06\mathrm{G}^{-0.7612} \quad (\mathrm{mm}^3/\mathrm{s}).$$

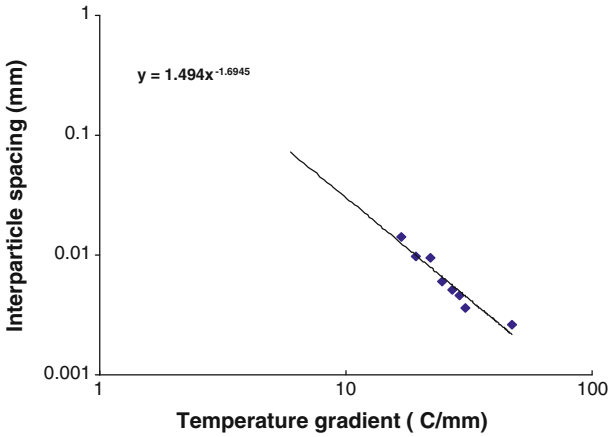

Fig. 13 Relationship between inter-particle spacing (λ) and temperature gradient (G) for Al–12%Si

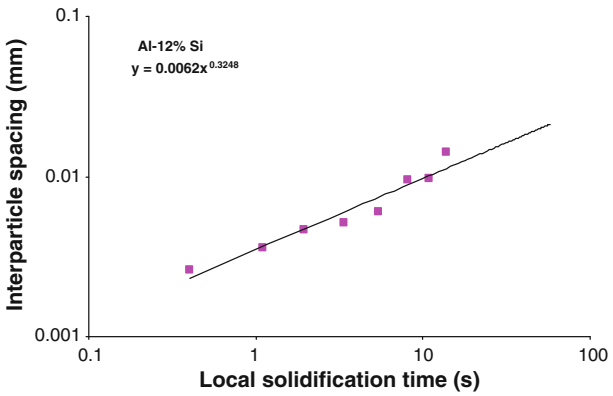

Fig. 14 Relationship between inter-particle spacing (λ) and local solidification time (t_f) for Al–12%Si

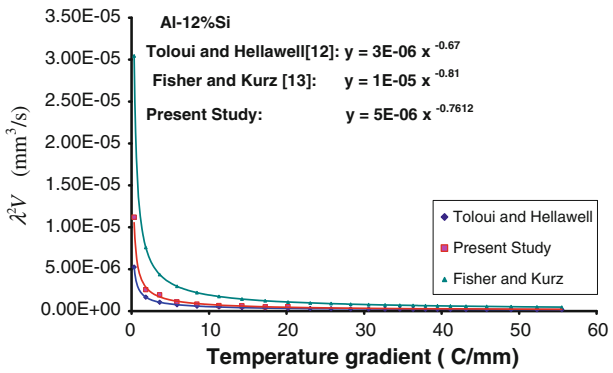

Fig. 15 Inter-particle spacing (λ), expressed as $\lambda^2 V$, as a function of the temperature gradient G, for Al–12%Si compared with previous studies

3. In the widely used Al–Si alloys the dispersion of the phases must reflect both decreasing growth rates and temperature gradient as the microstructure is examined from the chilled outer surface towards the interior of a casting. The increase in the coarseness of the microstructure is caused by both factors.
4. The lamellar spacing is strongly dependent on the interface velocity and an increase in growth rate causes refinement of the microstructure.
5. Measurements of inter-particle spacing (λ) in an unmodified Al–Si eutectic are in good agreement with the results of Toloui and Hellawell [12] and Fisher and Kurz [13].

6. The enthalpy transforming model proposed in this study is capable of handling complicated phase change problems occurring at a single temperature with fixed grids.

References

1. Sampath, R.: The adjoint method for the design of directional binary alloy solidification processes in the presence of a strong magnetic field. PhD Thesis, Cornell University, pp. 5–9 (2001)
2. Dantzig, J.A.: Multiscale methods, moving boundaries and inverse problems. IPAM Workshop on Tissue Engineering, University of Illinois, Urbana-Champaign (2003)
3. Elliot, R.; Glenister, S.M.D.: The growth temperature and interflake spacing in aluminum silicon eutectic alloys. Acta Metall. **28**, 1489–1494 (1980)
4. Borland, S.M.D.; Elliott, R.: Growth temperatures in Al–$CuAl_2$ and Sn–Cd eutectic alloys. Metall. Trans. A **9A**, 1063–1067 (1978)
5. Hogan, L.M.; Song, H.: Inter-particle spacing and undercoolings in Al–Si eutectic microstructures. Metall. Trans. A **18A**, 707–713 (1987)
6. Durbin, T.L.: Modeling dissolution in aluminum alloys. PhD Thesis, Georgia Institute of Technology, pp. 15–16 (2005)
7. Peres, M.D.; et al.: Macrostructure and microstructure development in Al–Si alloys directionally solidified under unsteady-state conditions. J. Alloys Compd. **381**, 168–181 (2004)
8. Chao, L.S.; Du, W.C.: Macro-micro modeling of solidification. Proc. Natl. Sci. Counc. Roc (A) **23**(5), pp. 622–629 (1999)
9. Mao, H.: A numerical study of external solidified products in the cold chamber die casting process. PhD. Thesis, The Ohio state University, pp. 8–22 (2004)
10. Cao, Y.; et al.: A numerical analysis of stefan problems for generalized multi-dimensional phase-change structures using the enthalpy transforming model. Int. J. Heat Mass Transf. **32**(7), pp. 1289–1298 (1989)
11. Ziolkowski, J.E.: Modeling of an aerospace sand casting process. MSc. Thesis, Worcester Polytechnic Institute, pp. 6–11 (2002)
12. Toloui, B.; Hellawell, A.: Phase separation and undercooling in Al–Si eutectic alloy—The influence of freezing rate and temperature gradient. Acta Metall. **24**, 565–573 (1976)
13. Fisher, D.J.; Kurz, W.: A theory of branching limited growth of irregular eutectics. Acta Metall. **28**, 777–794 (1980)